Surface Science 606 (2012) 181–185

Contents lists available at SciVerse ScienceDirect

Surface Science

journal homepage: www.elsevier.com/locate/susc

Ba and BaO_x surface structures on Au(111)

Chen Wu, Martin R. Castell *

Department of Materials, University of Oxford, Parks Road, Oxford, OX1 3PH, UK

ARTICLE INFO

Article history:
Received 16 June 2011
Accepted 18 September 2011
Available online 29 September 2011

Keywords:
Scanning tunneling microscopy
Epitaxy
Growth
Oxidation
Surface structure, morphology, roughness, and topography
Barium and barium oxide
Au(111) substrate

ABSTRACT

Scanning tunneling microscopy (STM) is used to investigate surface structures of barium and barium oxide grown on $(22\times\sqrt{3})$-reconstructed Au(111) surfaces. Evaporated Ba attaches to the Au herringbones after ultrahigh vacuum (UHV) annealing, forming a stripe pattern. Oxidation of the Ba stripes gives rise to a BaO_x structure pinned to the Au herringbones. Conversely, well-ordered epitaxial BaO_x structures can be obtained with oxidation of the deposited Ba by residual oxygen and subsequent UHV annealing. The two ordered BaO_x phases, a (6×6) and a $(2\sqrt{3}\times2\sqrt{3})$-$R30°$ structure, coexist on the surface and lift the Au reconstruction.

1. Introduction

Barium oxide is a material with applications in many technologically important areas including high current density cathodes [1-3], catalysts [4-6] and optical devices [7-9]. Most of these applications involve BaO layers in combination with other metal elements, which has stimulated investigations of BaO thin films on metals such as W(001) [10,11], W(110) [12,13], Ir(001) [14,15], Re(0001) [16,17] and Ni(110) [18-20]. The majority of these studies have focused on electronic and chemical characterization. Because the surface structures of BaO thin films partially determine the film properties and reflect the film–substrate interactions, a deeper understanding of the surface structure is necessary. Among the limited investigations in this area, Bowker et al. studied the surface structures of BaO grown on Pt(111) as an inverse catalyst model for NO_x reduction and storage and observed a (2×2) reconstruction of BaO [21-23]. Similarly, our studies of the growth of BaO thin films on Au(111) is partially motivated by the promoting effect of BaO on the catalytic properties of oxide supported Au nanoparticles [6,24-26]. Furthermore, BaO thin film growth on Au(111) enables surface science investigation of the BaO(111) face for two reasons. The first is that surface structure studies using electron-based techniques are difficult because BaO is an electrical insulator, but this restriction can be overcome by investigating thin films of BaO grown on a conducting substrate. This method is reviewed in Ref [27]. Secondly, the BaO(111) surface is polar and various mechanisms have been proposed for the stabilization of the polar surface, one of which is reconstruction [28]. The surface structure of the thin film form of BaO(111) is likely to be different to that of the bulk reconstruction because no macroscopic dipole can be created in the thin film to destabilize it [29].

In this paper, the growth of Ba and BaO_x films on reconstructed Au(111) surfaces is presented. Scanning tunneling microscopy (STM) offers insights into the surface structures and aids the understanding of the adsorption of Ba and its reactivity to O on metal substrates. Two well-ordered BaO_x phases are observed and their structures are discussed in the context of the experimental data combined with results from previous related studies [21,30-34].

2. Experimental methods

The experiments were carried out in a JEOL JSTM4500XT system, operating at a base pressure of 10^{-8} Pa. Mica-supported Au(111) single crystals (Agilent Technologies, UK) were used as the substrates. Details of the preparation method for clean reconstructed Au(111) substrates have been described elsewhere [35]. The resulting $(22\times\sqrt{3})$ reconstruction on the Au(111) surface was confirmed by STM prior to the deposition of Ba. Ba was deposited onto room temperature (RT) substrates in ultrahigh vacuum (UHV) from a getter wire (SAES Getters S.p.A.) installed in a dedicated Ba evaporator built in the Institute of Physics and Physical Technologies at the Technical University of Clausthal. Since Ba is highly reactive, it can be oxidized either by O_2 (10^{-6} Pa) purposefully introduced into the chamber or by the residual O in the chamber. In the latter case, the samples were annealed at approx. 450 °C in UHV to form ordered BaO_x structures. The amount of Ba deposited is estimated in monolayer (ML) equivalents, corresponding to the density of Au atoms per unit area of (1×1)-Au(111) (1.4×10^{15} atoms per cm^2).

* Corresponding author.
E-mail address: martin.castell@materials.ox.ac.uk (M.R. Castell).

0039-6028/$ – see front matter © 2011 Elsevier B.V. All rights reserved.
doi:10.1016/j.susc.2011.09.013

3. Results and discussion

3.1. Deposition and oxidation of Ba on Au(111)

The STM images in Fig. 1 show the as-deposited and oxidized barium on Au(111) surfaces. The Au(111) substrate surface forms a $(22 \times \sqrt{3})$ reconstruction with bright parallel rows that are the boundaries between the fcc and hcp regions. The surface has different domains rotated by 60° with respect to each other [36], resulting in a herringbone pattern as shown in Fig. 1a. Different domains are connected by elbow sites, containing surface dislocations caused by the 60° rotation of the two domains [37].

Fig. 1b shows an STM image of Ba islands and Au herringbones in the background, following 0.5 ML of Ba deposition. The as-deposited Ba forms islands randomly arranged on the Au(111) surface. This behavior is different from metals such as Fe [38-40], Co [41,42], Ni [43], Mn [44] and Ti [45,46] which preferentially nucleate at the elbow sites of the Au(111) surface and form regular arrays of islands. It has been found that the preferred nucleation site is determined by the surface energy of the deposited metal and the Au(111) surface [47]. Metals with higher surface energy than Au prefer to nucleate at the elbow sites while those with lower surface energy do not have this preference. A place-exchange mechanism has been proposed to explain this observation. It involves deposited metal atoms substituting for Au atoms in the substrate lattice and forming the nucleation sites for the further incoming deposits [47,48]. Ba(111) has a much lower surface energy (0.397 J/m^2) than that of Au(111) (1.283 J/m^2) [49], hence it can remain on the surface without substituting with the underlying Au atoms. The as-deposited Ba on Au(111) only forms islands with irregular shapes, indicating an incoherent interfacial relationship.

Even at RT Ba is mobile on the Au(111) surface. This can be seen in the STM image in Fig. 1c, taken within 10 min of Fig. 1b, where Ba has started to attach to the herringbones. The terrace height (approx. 2.4 Å) measured in Fig. 1c corresponds to the step height of the Au(111) lattice. The image also shows that Ba islands do not nucleate preferentially at the step edges.

After UHV annealing at 450 °C for 15 min, refined adhesion of the islands to the Au herringbones is observed in Fig. 1d, with stripes running along the directions of the three domains of the Au $(22 \times \sqrt{3})$ reconstruction. The distance measured between the stripes (64 ± 1 Å) matches the distance between the Au herringbones (63 Å). As Ba is highly reactive, the deposited Ba may by this stage have partially reacted with the residual O in the chamber to form BaO_x islands.

Following further annealing at 450 °C for 45 min, the islands spread over the substrate surface as shown in Fig. 1e where their alignment with the domains of the Au substrate is still visible. At this stage, the sample has been kept in the chamber for 72 h. The STM image (Fig. 1e) appears very similar to Fig. 1f, which was obtained after annealing the sample in 10^{-6} Pa O_2 for 30 min followed by UHV annealing at 450 °C. The similarity between the two STM images indicates that the sample left in-situ for 72 h has already been oxidized by residual O as a result of the strong reactivity of Ba.

3.2. Reconstructions of BaO_x on Au(111)

As demonstrated in the previous section, the deposited Ba can be oxidized either by the residual O in the chamber or by purposefully introduced O_2. With introduced O_2 at a relatively high pressure (10^{-6} Pa), no ordered BaO structure was observed. To obtain epitaxial BaO_x structures on the Au(111) substrate, deposited Ba (0.4 ML) was oxidized by residual O in the chamber over 72 h prior to UHV annealing at 450 °C for 15 min. This leads to the coexistence of three structures marked 'α', 'β' and 'γ' as shown in Fig. 2. The image is high pass filtered so that the steps are flattened and various

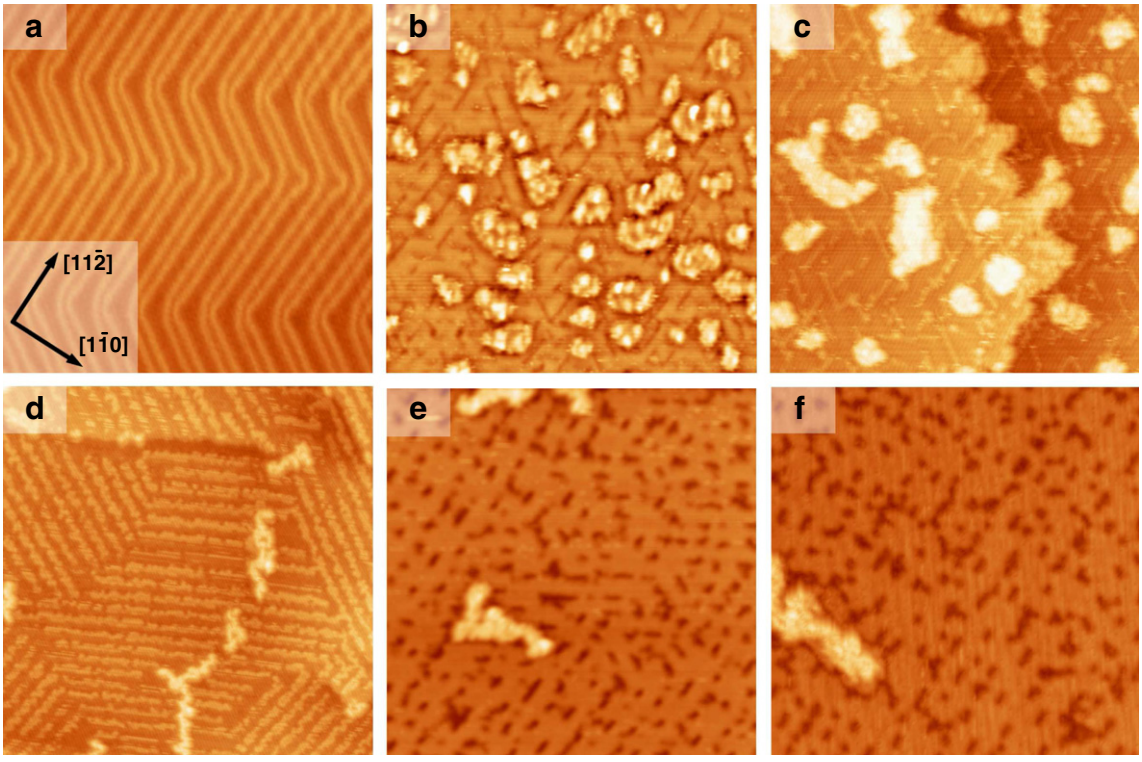

Fig. 1. STM images showing (a) a $(22 \times \sqrt{3})$-reconstructed Au(111) surface as the substrate for Ba deposition (Image size: 79 × 79 nm^2, $V_s = -1.83$ V, $I_t = 0.20$ nA); (b) Ba islands grown following Ba deposition onto the RT Au(111) surface (image size: 81 × 81 nm^2, $V_s = -1.91$ V, $I_t = 0.20$ nA); (c) Ba islands surrounded by a small amount of Ba attaching to the Au herringbones (image size: 92 × 92 nm^2, $V_s = -1.00$ V, $I_t = 0.20$ nA); (d) stripes running along the three directions of the Au reconstruction after UHV annealing at 450 °C for 15 min (image size: 121 × 121 nm^2, $V_s = -0.53$ V, $I_t = 0.20$ nA); (e) BaO_x layer spreading over the Au(111) substrate surface following further UHV annealing at 450 °C for 45 min with the sample being kept in-situ for 72 h (Image size: 64 × 64 nm^2, $V_s = -1.00$ V, $I_t = 0.20$ nA); (f) similar morphology as in (e) after first annealing in 10^{-6} Pa O_2 and then in UHV (Image size: 64 × 64 nm^2, $V_s = -0.99$ V, $I_t = 0.20$ nA).

structures with different heights can be shown on the same image. Structure γ is only observed covering a few percent of the surface area and appears disordered. It is possible that this structure is an intermediate phase. The other two structures, α and β, are well-ordered over larger surface areas. The angle between the two close packed directions of the ordered structures is measured as 30°. Fig. 2b and c show line profiles measured along arrows 'i' and 'ii', indicating that structure β is approx. 1.8 Å higher than γ, while the difference of the apparent height between structure α and β is approx. 0.9 Å.

Although the images in Fig. 1e, f and 2 all show BaO_x surface structures on the Au(111) surface, Fig. 2 exhibits rather different morphologic features. As can be seen from the evolution in Fig. 1b–d, Ba tends to wet the substrate surface because it has a significantly lower surface energy than Au(111). UHV annealing immediately following Ba deposition facilitates the spread of Ba and its adhesion to the Au herringbones. As a result, the formed BaO_x islands stay pinned to the nucleation sites of Ba after oxidation (Fig. 1e and f). In contrast, not having the annealing process prior to oxidation allows the as-deposited Ba to be oxidized before it has adhered to the Au herringbones. Consequently, the formed BaO_x does not stay pinned and this allows the formation of well-ordered BaO_x structures with subsequent annealing (Fig. 2).

Fig. 3a shows an STM image of structure α with a unit cell indicated. The structure is composed of bright spots forming a hexagonal lattice that lifts the Au(111) reconstruction. Arrows marked as 'i' and 'ii' denote

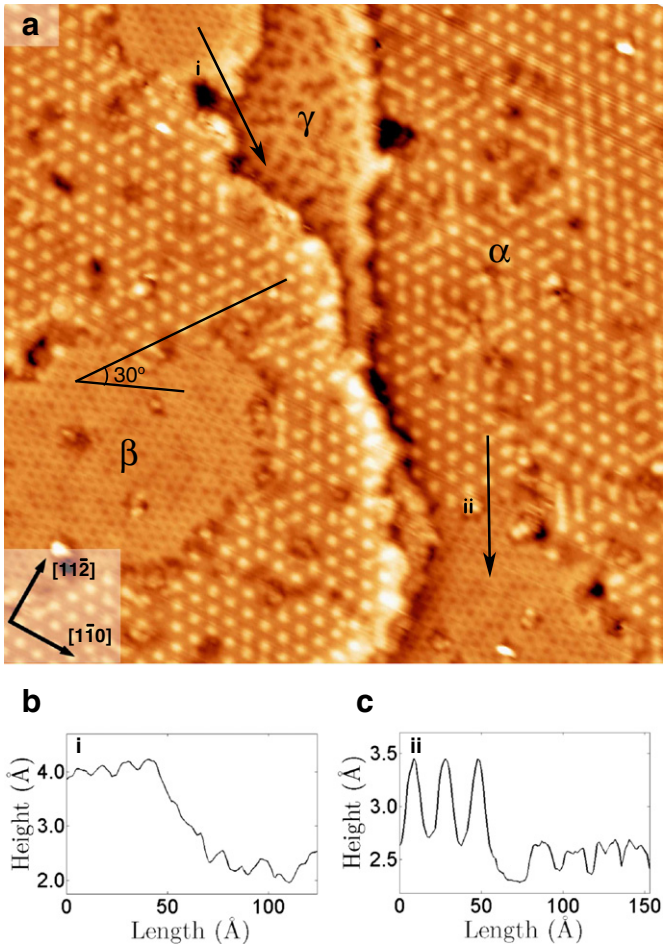

Fig. 2. (a) STM image (high pass filtered) that shows the coexistence of BaO_x structures of well-ordered α and β, as well as disordered γ phases. The two epitaxial BaO_x structures are rotated by an angle of 30° with respect to each other. (Image size: 74×74 nm^2, V_s = −1.68 V, I_t = 0.20 nA.). (b) and (c) profiles taken along arrows marked as 'i' and 'ii' in (a).

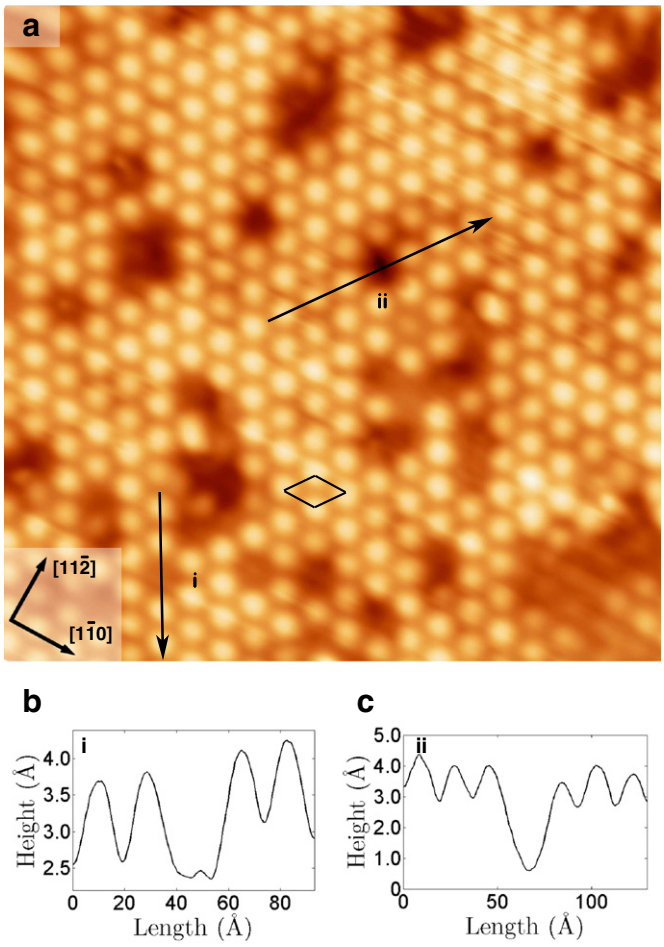

Fig. 3. (a) STM image showing the (6×6) hexagonal BaO_x structure with a unit cell indicated (image size: 36×36 nm^2, V_s = 1.26 V, I_t = 0.20 nA). (b) and (c) profiles taken along arrows marked as 'i' and 'ii' in (a).

the line profiles shown in Fig. 3b and c. A periodicity of 17.6 ± 0.4 Å is measured along the close packed directions. The hexagonal BaO_x structure is aligned with the crystallographic directions of the Au substrate. Thus, a (6×6) reconstruction can be determined with the atomic spacing of the Au(111) lattice being 2.89 Å. The BaO_x surface contains a number of defect sites where the bright spots are missing. Measuring the depth of the defect sites provides an indication of the thickness of the (6×6) BaO_x structure on Au(111). The depth of the defect site in Fig. 3b is approx. 1.3 Å, while Fig. 3c shows a larger depth (approx. 3.8 Å), indicating that the (6×6) BaO_x structure on Au(111) is probably a multi-layer phase.

Structure β exhibits a honeycomb structure composed of edge-sharing hexagons, one of which is indicated in Fig. 4a. A unit cell is also indicated in the image, which is formed by connecting the centers of the hexagons. The line profiles shown in Fig. 4b and c are taken along arrows marked as 'i' and 'ii'. A periodicity of 10.2 ± 0.3 Å is measured in Fig. 4b. The honeycomb BaO_x structure is rotated by 30° with respect to the (6×6) BaO_x structure which aligns with the Au(111) lattice (Fig. 2). Consequently, a $(2\sqrt{3}\times 2\sqrt{3})$-*R*30° reconstruction can be determined for the honeycomb BaO_x structure on the Au(111) surface. The reconstruction will be referred as $(2\sqrt{3}\times 2\sqrt{3})$ for simplicity. The edges of the hexagons of the BaO_x honeycomb structure consist of two adjacent bright spots, the spacing between them is approx. 5.9 Å as shown in Fig. 4c. Although the $(2\sqrt{3}\times 2\sqrt{3})$ BaO_x structure has a regular periodicity, the brightness of the structure appears uneven, and the background resembles the appearance of the disordered γ phase in Fig. 2. It is therefore possible that the $(2\sqrt{3}\times 2\sqrt{3})$ BaO_x structure grows on top of the γ

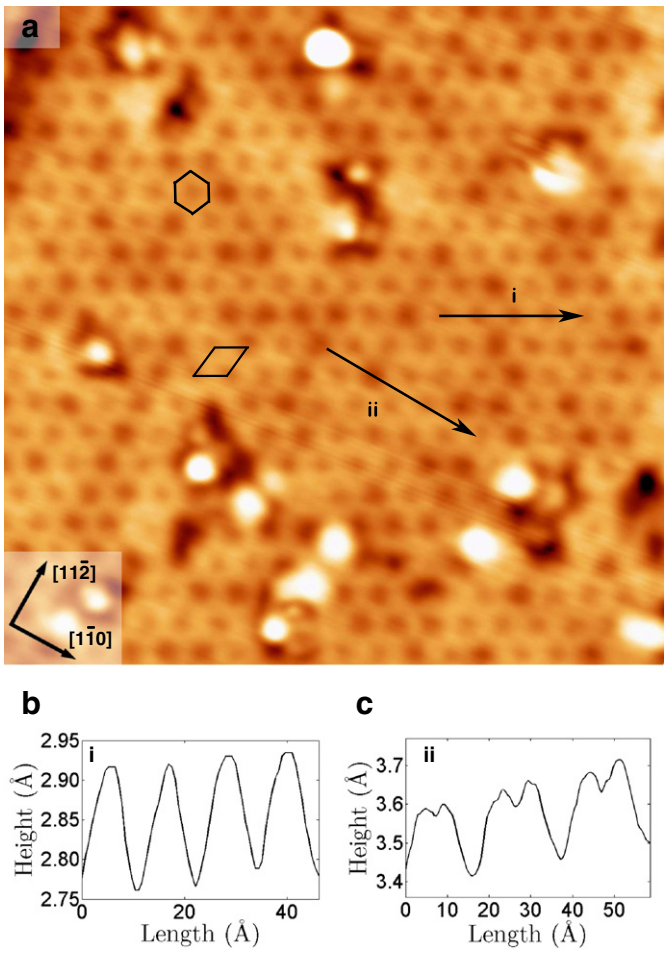

Fig. 4. (a) STM image of the honeycomb BaO_x structure composed of edge-sharing hexagons. The centers of the hexagons form $(2\sqrt{3}\times2\sqrt{3})$ unit cells, one of which is indicated in the image (image size: 22×22 nm^2, $V_s=-1.68$ V, $I_t=0.20$ nA). (b) and (c) profiles taken along arrows marked as 'i' and 'ii' in (a).

phase. This is supported by the fact that the former is measured as approx. 1.8 Å higher than the latter on the same image (Fig. 2).

3.3. Structural models

Although there are limited structure studies on BaO surfaces, the (111) crystal facets of similar rock-salt metal oxides (MO) such as VO [50-53], FeO [30,54-58], NiO [59,60,32], MgO [33,61-64], MnO [31,65,66] and CoO [42,67] have been investigated due to the interest in polar crystal terminations. It is instructive to compare our results of the BaO_x phases on Au(111) to previous studies to gain a better understanding of the possible structures. Various models have been proposed for the hexagonal MO(111) surface reconstructions in the literature including Moiré patterns, cyclic ozone structures, octopole based structures and hydroxylated structures. Most of these models involve mechanisms to stabilize the polar surface. However, for ultrathin films the dipole can be compensated by the interface dipole induced by charge transfer between the metal substrate and oxide overlayer [68,69]. Consequently, there is not necessarily a need for dipole cancellation in ultrathin films.

A Moiré pattern involves superpositioning one lattice on another. It has been used to explain a pinwheel structure observed on VO/Rh(111) [52,53] as well as honeycomb and hexagonal structures obtained on FeO/Pt(111) [30,55-58]. Oxygen atoms are located at the three-fold hollow sites of the V/Fe layer, forming a stoichiometric MO bilayer. The nature of the Moiré pattern results in two different periodicities that are observed with STM: a relatively long periodicity for the coincident sites and a short atomic periodicity for the surface layer. Meanwhile, different occupation sites of the MO layer usually lead to different heights of the atoms, and hence different levels of brightness in STM images. The height difference for Moiré patterns in STM images is usually very small ($\leq$0.5 Å), as the atoms being imaged are all in the same layer. As shown in Fig. 3a, the (6×6) reconstruction of BaO_x on Au(111) has a corrugation height of approx. 1 Å, which almost corresponds to the thickness of an atomic layer and is probably too large to be due to a Moiré pattern. As for the $(2\sqrt{3}\times2\sqrt{3})$ BaO_x structure on Au(111), it appears uneven across the surface due to the disordered layer underneath which is unlikely to induce the coincident sites required by the Moiré pattern.

The second type of model proposed for the MO(111) surface reconstruction involves a cyclic ozone structure, which contains oxygen trimers around an M atom and isolated M atoms. It has been found that such a structure does not cancel the divergence of dipoles efficiently and the oxygen trimers dissociate upon full geometric relaxation, converting the initial hexagonal structure into a stripe structure [31]. The M atoms surrounded by the oxygen trimers would be expected to have different brightness to those isolated ones in STM images, which is not observed for both BaO_x structures on Au(111).

The octopolar model has a pyramid shape with {001} facets. The structure can be either O- or M-terminated with an M or O triangular base [70]. The octopolar model has been proposed for the (2×2)-reconstructed NiO(111) surface [32,59,60,71], $(\sqrt{3}\times\sqrt{3})$-*R*30° MnO (111) reconstruction [66] and the (2×2) BaO structure on Pt(111) [21]. Theoretical calculations predict that the formation of facets allows the dipole moments to cancel out along the three orthogonal axes [32,60], which serves as an efficient way of forming stable surface structures for rock-salt crystals. One might expect that for an octopolar structure there will be lateral displacements of the pyramids, especially in the (6×6) reconstruction. However, we only observe regular periodicities which indicate that an octopolar reconstruction is unlikely.

Hydroxylated structures have been suggested for (1×1), (2×2) and $(\sqrt{3}\times\sqrt{3})$-*R*30° reconstructions on the MgO(111) surface [33,63,64] and (2×2) and $(\sqrt{3}\times\sqrt{3})$-*R*30° NiO(111) reconstructions [34]. Since the structures presented here are produced via Ba oxidation with the residual O-containing species mainly being water, it is likely that hydroxyl groups will bond onto the surface. The STM images possibly reveal the hydroxide structure rather than the naked oxide surface. At this stage, it is difficult to propose precise structural models that take hydroxylation into account. Further studies such as analysis of low energy electron diffraction (LEED) intensity–voltage curves and theoretical calculations would be useful to further add to the determination of the surface structures.

4. Conclusions

Ba has been deposited onto reconstructed Au(111) surfaces and oxidized by residual O in the chamber. Annealing the deposited Ba in UHV facilitates its adhesion to the Au herringbones and forms a stripe pattern which is aligned with the three domains of the Au reconstruction. The attached Ba stays pinned after oxidation. Epitaxial BaO_x structures can be obtained by oxidation of deposited Ba with residual O and subsequent UHV annealing. Two well-ordered BaO_x structures have been observed coexisting on the same surface. They correspond to a (6×6) and a $(2\sqrt{3}\times2\sqrt{3})$ BaO_x structure on Au(111). While very few studies have been reported on the bulk BaO(111) surface reconstruction due to the insulating nature of BaO, the epitaxial ultrathin film structures reported here are likely to be different from bulk BaO(111) terminations because of the influence of the Au(111) substrate. Further surface structure experiments in combination with theoretical modeling is necessary to determine the detailed atomic structure of the ultrathin films.

Acknowledgments

The authors thank Chris Spencer (JEOL, UK) for valuable technical support, and Dr. Wolfgang Maus-Friedrichs and Karen Kruska for their involvement in building the Ba evaporator.

References

[1] A. Shih, J.E. Yater, C. Hor, Appl. Surf. Sci. 242 (2005) 35.
[2] A.A. Hashim, A.K. Ray, A.K. Hassan, D.S. Barratt, Appl. Surf. Sci. 243 (2005) 421.
[3] R. Forman, J. Appl. Phys. 47 (2009) 5272.
[4] P. Stone, M. Ishii, M. Bowker, Surf. Sci. 537 (2003) 179.
[5] R.D. Clayton, M.P. Harold, V. Balakotaiah, Appl. Catal., B 81 (2008) 161.
[6] B.P.C. Hereijgers, B.M. Weckhuysen, ChemSusChem 2 (2009) 743.
[7] J.L. Wu, C.M. Wang, G.M. Zhang, J. Appl. Phys. 83 (1998) 7855.
[8] J.L. Wu, Q.F. Zhang, C.M. Wang, Y.H. Zou, Appl. Surf. Sci. 183 (2001) 80.
[9] H. Yang, L. Ma, X.B. Xie, H.F. Yu, Phys. Lett. A 348 (2006) 272.
[10] A. Lamouri, W. Muller, I.L. Krainsky, Phys. Rev. B: Condens. Matter 50 (1994) 4764.
[11] J. Almanstötter, T. Fries, B. Eberhard, J. Appl. Phys. 86 (1999) 325.
[12] D.R. Mueller, R.L. Kurtz, R.L. Stockbauer, T.E. Madey, A. Shih, Surf. Sci. 237 (1990) 72.
[13] I.-H. Hong, C.-P. Cheng, T.-W. Pi, Surf. Sci. 601 (2007) 1726.
[14] G.A. Haas, A. Shih, R.E. Thomas, Appl. Surf. Sci. 1 (1977) 59.
[15] G.A. Haas, C.R. Marrian, A. Shih, Appl. Surf. Sci. 16 (1983) 125.
[16] D.A. Gorodets, A.N. Knysh, Surf. Sci. 40 (1973) 636.
[17] D.A. Gorodets, A.N. Knysh, Surf. Sci. 40 (1973) 651.
[18] D. Vlachos, M. Kamaratos, S.D. Foulias, J. Phys. Condens. Matter 18 (2006) 6997.
[19] D. Vlachos, S.D. Foulias, M. Kamaratos, Synth. React. Inorg. Met.-Org. Nano-Metal. Chem. 38 (2008) 400.
[20] D. Vlachos, S.D. Foulias, M. Kamaratos, J. Phys. Condens. Matter 21 (2009) 445004.
[21] M. Bowker, P. Stone, R. Smith, E. Fourre, M. Ishii, N.H. de Leeuw, Surf. Sci. 600 (2006) 1973.
[22] M. Bowker, M. Cristofolini, M. Hall, E. Fourre, F. Grillo, E. McCormack, P. Stone, M. Ishii, Top. Catal. 42–43 (2007) 341.
[23] M. Bowker, Chem. Soc. Rev. 37 (2008) 2204.
[24] A.C. Gluhoi, X. Tang, P. Marginean, B.E. Nieuwenhuys, Top. Catal. 39 (2006) 101.
[25] A.C. Gluhoi, B.E. Nieuwenhuys, Catal. Today 122 (2007) 226.
[26] V.R. Choudhary, D.K. Dumbre, Top. Catal. 52 (2009) 1677.
[27] N. Nilius, Surf. Sci. Rep. 64 (2009) 595.
[28] C. Noguera, J. Phys. Condens. Matter 12 (2000) R367.
[29] J. Goniakowski, F. Finocchi, C. Noguera, Rep. Prog. Phys. 71 (2008) 016501.
[30] W. Ranke, M. Ritter, W. Weiss, Phys. Rev. B 60 (1999) 1527.
[31] C. Franchini, V. Bayer, R. Podloucky, G. Parteder, S. Surney, F.P. Netzer, Phys. Rev. B 73 (2006) 155402.
[32] W.B. Zhang, B.Y. Tang, J. Chem. Phys. 128 (2008) 124703.
[33] J. Ciston, A. Subramanian, L.D. Marks, Phys. Rev. B 79 (2009) 085421.
[34] J. Ciston, A. Subramanian, D.M. Kienzle, L.D. Marks, Surf. Sci. 604 (2010) 155.
[35] C. Wu, M.S.J. Marshall, M.R. Castell, J. Phys. Chem. C 115 (2011) 8643.
[36] F. Silly, A.Q. Shaw, G.A.D. Briggs, M.R. Castell, Appl. Phys. Lett. 92 (2008) 023102.
[37] J.V. Barth, H. Brune, G. Ertl, R.J. Behm, Phys. Rev. B 42 (1990) 9307.
[38] B. Voigtlander, G. Meyer, N.M. Amer, Surf. Sci. 255 (1991) L529.
[39] J.A. Stroscio, D.T. Pierce, R.A. Dragoset, P.N. First, J. Vac. Sci. Technol., A 10 (1992) 1981.
[40] N.A. Khan, C. Matranga, Surf. Sci. 602 (2008) 932.
[41] B. Voigtlander, G. Meyer, N.M. Amer, Phys. Rev. B 44 (1991) 10354.
[42] I. Sebastian, M. Heiler, K. Meinel, H. Neddermeyer, Appl. Phys. A: Mater. Sci. Process. 66 (1998) S525.
[43] D.D. Chambliss, R.J. Wilson, S. Chiang, J. Vac. Sci. Technol. B 9 (1991) 933.
[44] M. Fonin, Y.S. Dedkov, U. Rudiger, G. Guntherodt, Surf. Sci. 529 (2003) L275.
[45] J. Biener, E. Farfan-Arribas, M. Biener, C.M. Friend, R.J. Madix, J. Chem. Phys. 123 (2005) 094705.
[46] D.V. Potapenko, R.M. Osgood, Nano Lett. 9 (2009) 2378.
[47] J.A. Meyer, I.D. Baikie, E. Kopatzki, R.J. Behm, Surf. Sci. 365 (1996) L647.
[48] C.S. Casari, S. Foglio, F. Siviero, A. Li Bassi, M. Passoni, C.E. Bottani, Phys. Rev. B 79 (2009) 195402.
[49] L. Vitos, A.V. Ruban, H.L. Skriver, J. Kollar, Surf. Sci. 411 (1998) 186.
[50] M. Petukhov, G.A. Rizzi, G. Granozzi, Thin Solid Films 400 (2001) 154.
[51] S. Surnev, M.G. Ramsey, F.P. Netzer, Prog. Surf. Sci. 73 (2003) 117.
[52] J. Schoiswohl, M. Sock, S. Eck, S. Surnev, M.G. Ramsey, F.P. Netzer, G. Kresse, Phys. Rev. B 69 (2004) 155403.
[53] J. Schoiswohl, S. Surnev, M. Stock, S. Eck, M.G. Ramsey, F.P. Netzer, Phys. Rev. B 71 (2005) 165437.
[54] E.D.L. Rienks, N. Nilius, H.-P. Rust, H.-J. Freund, Phys. Rev. B 71 (2005) 241404(R).
[55] L. Giordano, G. Pacchioni, J. Goniakowski, N. Nilius, D.L.R. Emile, H.-J. Freund, Phys. Rev. B 76 (2007) 075416.
[56] L.R. Merte, J. Knudsen, L.C. Grabow, R.T. Vang, E. Laegsgaard, M. Mavrikakis, F. Besenbacher, Surf. Sci. 603 (2009) L15.
[57] W. Zhang, Z. Li, Y. Luo, J. Yang, J. Phys. Chem. C 113 (2009) 8302.
[58] J. Knudsen, L.R. Merte, L.C. Grabow, F.M. Eichhorn, S. Porsgaard, H. Zeuthen, R.T. Vang, E. Laegsgaard, M. Mavrikakis, F. Besenbacher, Surf. Sci. 604 (2010) 11.
[59] A. Barbier, C. Mocuta, H. Kuhlenbeck, K.F. Peters, B. Richter, G. Renaud, Phys. Rev. Lett. 84 (2000) 2897.
[60] C.A.J. Fisher, Scr. Mater. 50 (2004) 1045.
[61] G.W. Watson, E.T. Kelsey, N.H. de Leeuw, D.J. Harris, S.C. Parker, J. Chem. Soc. 92 (1996) 433.
[62] A. Pojani, F. Finocchi, J. Goniakowski, C. Noguera, Surf. Sci. 387 (1997) 354.
[63] V.K. Lazarov, R. Plass, H.C. Poon, D.K. Saldin, M. Weinert, S.A. Chambers, M. Gajdardziska-Josifovska, Phys. Rev. B 71 (2005) 115434.
[64] H.C. Poon, X.F. Hu, S.E. Chamberlin, D.K. Saldin, C.J. Hirschmugl, Surf. Sci. 600 (2006) 2505.
[65] G.A. Rizzi, M. Petukhov, M. Sambi, R. Zanoni, L. Perriello, G. Granozzi, Surf. Sci. 482–485 (2001) 1474.
[66] F. Allegretti, C. Franchini, V. Bayer, M. Leitner, G. Parteder, B. Xu, A. Fleming, M.G. Ramsey, R. Podloucky, S. Surnev, F.P. Netzer, Phys. Rev. B 75 (2007) 224120.
[67] S. Sindhu, M. Heiler, K.M. Schindler, H. Neddermeyer, Surf. Sci. 541 (2003) 197.
[68] J. Goniakowski, C. Noguera, Phys. Rev. B 79 (2009) 155433.
[69] J. Goniakowski, L. Giordano, C. Noguera, Phys. Rev. B 81 (2010) 205404.
[70] D. Wolf, Phys. Rev. Lett. 68 (1992) 3315.
[71] C.A. Ventrice, T. Bertrams, H. Hannemann, A. Brodde, H. Neddermeyer, Phys. Rev. B 49 (1994) 5773.